Shock Waves (2014) 24:21–32
DOI 10.1007/s00193-013-0457-4

ORIGINAL ARTICLE

# Experimental exploration of underexpanded supersonic jets

**Benoît André · Thomas Castelain · Christophe Bailly**

Received: 28 October 2011 / Revised: 17 December 2012 / Accepted: 17 February 2013 / Published online: 2 July 2013


**Abstract** Two underexpanded free jets at fully expanded Mach numbers $M_j = 1.15$ and 1.50 are studied. Schlieren visualizations as well as measurements of static pressure, Pitot pressure and velocity are performed. All these experimental techniques are associated to obtain an accurate picture of the jet flow development. In particular, expansion, compression and neutral zones have been identified in each shock cell. Particle lag is considered by integrating the equation of motion for particles in a fluid flow and it is found that the laser Doppler velocimetry is suitable for investigating shock-containing jets. Even downstream of the normal shock arising in the $M_j = 1.50$ jet, the measured gradual velocity decrease is shown to be relevant.

**Keywords** Supersonic jet · Shock-cell structure · Laser Doppler velocimetry · Particle lag · Pressure measurements

Communicated by A. K. Hayashi and K. Kontis.

The paper was based on work that was presented at the 28th International Symposium on Shock Waves, 17–22 July.

B. André · T. Castelain (✉) · C. Bailly
Laboratoire de Mécanique des Fluides et d'Acoustique,
UMR CNRS 5509, Ecole Centrale de Lyon, Université de Lyon,
36 Avenue Guy de Collongue, 69134 Ecully Cedex, France
e-mail: thomas.castelain@ec-lyon.fr

T. Castelain
Université Lyon 1, 43 Boulevard du 11 Novembre 1918,
69622 Villeurbanne Cedex, France

C. Bailly
Institut Universitaire de France, Paris, France

## 1 Introduction

Underexpanded jets have been studied for a long time in aeronautics. The nozzle pressure ratio (henceforth NPR), defined as the ratio of upstream stagnation pressure to ambient pressure, must be above a critical value to get an underexpanded jet. With the assumption of isentropic, one-dimensional flow, this critical value is expressed as $[(\gamma + 1)/2]^{\gamma/(\gamma-1)}$ for a convergent nozzle and is near 1.89 for air ($\gamma$ is the ratio of specific heats of the gas). The jet being underexpanded means that the static pressure at the nozzle exit is higher than the ambient. The pressure mismatch generates a quasi-periodic shock-cell pattern [20]. The pioneering studies mainly focused on the structure of highly underexpanded flows, featuring a so-called barrel shock and a large Mach disc (see, e.g., [1,12]). More detailed investigations of local mean values taken by important flow variables, such as velocity, static pressure or Mach number, defined by the ratio of local velocity to local speed of sound, were also performed. Donaldson and Snedecker [6] measured the impact pressure in two supersonic jets, with and without Mach disc. Seiner and Norum [25] and Hu and McLaughlin [9] deduced Mach number profiles from static and Pitot pressure measurements. However, the absence of comparison with flow visualizations makes the picturing of the shock-cell structure difficult. Norum and Seiner [18] led extensive static pressure measurements on the jet centreline and off axis in an attempt to link shock-cell structure to shock-associated noise; these measurements were compared to mean flow simulations by Seiner et al. [24]. Katanoda et al. [10] measured Pitot pressures in jets with Mach disc and compared them to numerical simulations. Laser Doppler velocimetry (LDV) was applied by Eggins and Jackson [7] in a choked jet at NPR = 6.6 containing a Mach disc and by Nouri and Whitelaw [19] at NPR = 3.6

without one. Bridges and Wernet [5] applied time-resolved particle image velocimetry to shock-containing hot jets to study the turbulence associated with broadband shock-associated noise. Finally, Panda and Seasholtz [20] used the Rayleigh scattering technique to perform very detailed density measurements in jets at several degrees of underexpansion. In the first two shock cells, they compared radial traverses with schlieren images to obtain an accurate picture of the shock-cell structure.

Hence, measurements of velocity and Mach number evolution in shock-containing jet plumes are scarce. The purpose of this contribution is to associate pressure measurements, LDV and schlieren images of underexpanded jets to achieve a clearer picture of the development of these jets and link measured features with patterns from the flow visualization. This paper is organised as follows: The experimental set-up is presented in Sect. 2. The important issue of particle lag is addressed in Sect. 3. Finally, results are displayed and discussed in Sect. 4 for two underexpanded jets.

## 2 Experimental set-up

In this study, the supersonic flow originates from a continuously operating compressor mounted upstream of an air drier. The jet exhausts through a $D = 38.25$ mm diameter contoured convergent nozzle. The NPR is set by measuring the wall static pressure fifteen nozzle diameters upstream of the exit. The stagnation pressure is retrieved from the static pressure value using a local Mach number estimate in the measuring section, which is known by the use of the area Mach number relation (see, e.g., [2]). The reservoir temperature $T_t$ is also measured upstream of the exit. In the following, results for unheated jets of ideally expanded Mach numbers $M_j = 1.15$ and 1.50 are presented, corresponding to NPR = 2.27 and 3.67, respectively.

A conventional $Z$-type schlieren system is used to visualise the flow. It consists of a continuous QTH light source, two $f/8$ parabolic mirrors with diameter of 203.2 mm, a straight knife-edge set perpendicular to the flow direction and a high-speed CMOS camera. Mean pictures are computed from a large collection of short-exposure images.

Measuring static pressure ($P_s$) in a shock-containing jet is no obvious undertaking. Some of the difficulties arising are that the orientation of the local velocity vector is not uniform in the flow and that the probe generates a shock upstream of it, which modifies the pressure field. A short static pressure probe design rather insensitive to the angle of attack was proposed by Pinckney [22]. The one built for this study follows a slight modification of the quoted design made by Norum and Seiner [18]. It has an outer diameter of 1.5 mm and a tip to static hole distance of about 4.5 mm. Results for the jet centreline have been compared to profiles from [18] and a good agreement has been found. The Pitot pressure ($P_p$) probe consists in a 1.5 mm outer diameter stainless steel tubing cut square.

The flow velocity is measured by LDV. An Argon ion Spectra-Physics 2017 laser operates on the green line of wavelength 514.50 nm with a power of 100 mW. The optical arrangement provides a measurement volume of approximately 1.5 mm length and 100 μm diameter. The fringes are set perpendicular to the jet axis so that the axial velocity component is measured. It implies that the long measurement volume dimension is perpendicular to the axis. The receiving optics collects the forward scattered Doppler bursts approximately 30° off axis. The Doppler signals are finally analysed by a BSA F80 processor with a clock frequency of 180 MHz. The flow is seeded with olive oil by means of Laskin nozzle generators. The mean particle size is known to be around 1 μm. No seeding of the jet surroundings has been set up but the measurements presented next mostly remain within the jet potential core and the first two nozzle diameters so this is not expected to lead to large velocity overestimations. The ensemble averages are performed over at least 100,000 individual velocity realizations (but usually much more) acquired over approximately 10 s. The simplified one-dimensional correction procedure of McLaughlin and Tiederman [14] as well as the weighting function of Barnet and Bentley [3] have been tested for the estimation of unbiased mean velocities. As expected, the correction is very small (about 0.1%) as long as the turbulence intensity is small, which is the case for the most part of the data presented in the following. The correction becomes significant for a very limited number of data points behind the Mach disc at $M_j = 1.50$, where it is of the order of a few percent of the raw velocity. But it has been observed at these locations that the two correction techniques had opposite trends. As a consequence, no biasing correction has been applied and the mean velocity is computed as the arithmetic mean of the velocity realizations.

## 3 Response of the seeding particles to the flow

One well-known disadvantage of laser Doppler velocimetry arises from the necessity of seeding the flow to acquire velocity signals. One actually measures the particle velocity instead of the fluid velocity and therefore, the measurement accuracy is limited by the ability of the particles to follow the flow. In the case of a shock-containing jet, the high velocity gradients through the shock cells make it even more difficult. An experimental observation of particle lag and a numerical procedure for estimating its effect are presented in the following.

### 3.1 Experimental observation of particle lag

The phenomenon of particle lag has been identified on acquired velocity signals and steps have been undertaken to reduce it. Some velocity histograms at different axial stations for $M_j = 1.15$ with different acquisition settings are presented in Fig. 1. In the top row, the photomultiplier feeding voltage is relatively low and the mean acquisition frequency is about 20 kHz, whereas the voltage has been raised for the acquisition displayed in the lower row, leading to a mean sample rate of about 120 kHz. In both acquisitions, particle lag is visible as an asymmetry on the histograms. When the flow is accelerating (left column), a small bump appears on the side of lower velocities. At the beginning of the compression zone (centre), when the flow starts decelerating, the histogram is symmetric. Further in the compression region (right column), a small fraction of particles travels at a higher velocity than the bulk. Raising the photomultiplier feeding voltage is seen to reduce the phenomenon of lag, if not suppress it, as is noticeable in Fig. 1. It is believed that the visibility of small oil droplets is thus enhanced. Validation rates typically above 90% ensure that the acquired Doppler bursts are not altered by this process.

The observation of velocity histograms can only show that just a small number of particles is not following the bulk, but still nothing is known about the velocity bias due to the finite mean particle size. An analytical model for particle motion has thus been applied.

### 3.2 Numerical integration of the particle behaviour

Several investigations addressed the question of the behaviour of seeding particles for both LDV or particle image velocimetry (PIV). For instance, Yanta et al. [28] looked experimentally and numerically into the application of LDV to supersonic flows. Particle lag was considered in their work with respect to both turbulence and strong gradients. They highlighted the importance of having very small and well calibrated particles. Ross et al. [23] evaluated numerically the relaxation distance of seeding particles of known diameter. By comparing the predicted relaxations to PIV results, they could deduce the particle diameter. They finally applied PIV to a shock-containing jet and stated that the error induced by the particle lag does not exceed the accuracy of the method except in areas just downstream of shocks. Melling [15], in his review of seeding material usually used in PIV experiments in connection with that particular problem, presents the Basset equation of motion for a small spherical solid particle in a surrounding medium in the case of a single-phase flow, which means that the particle concentration needs to be

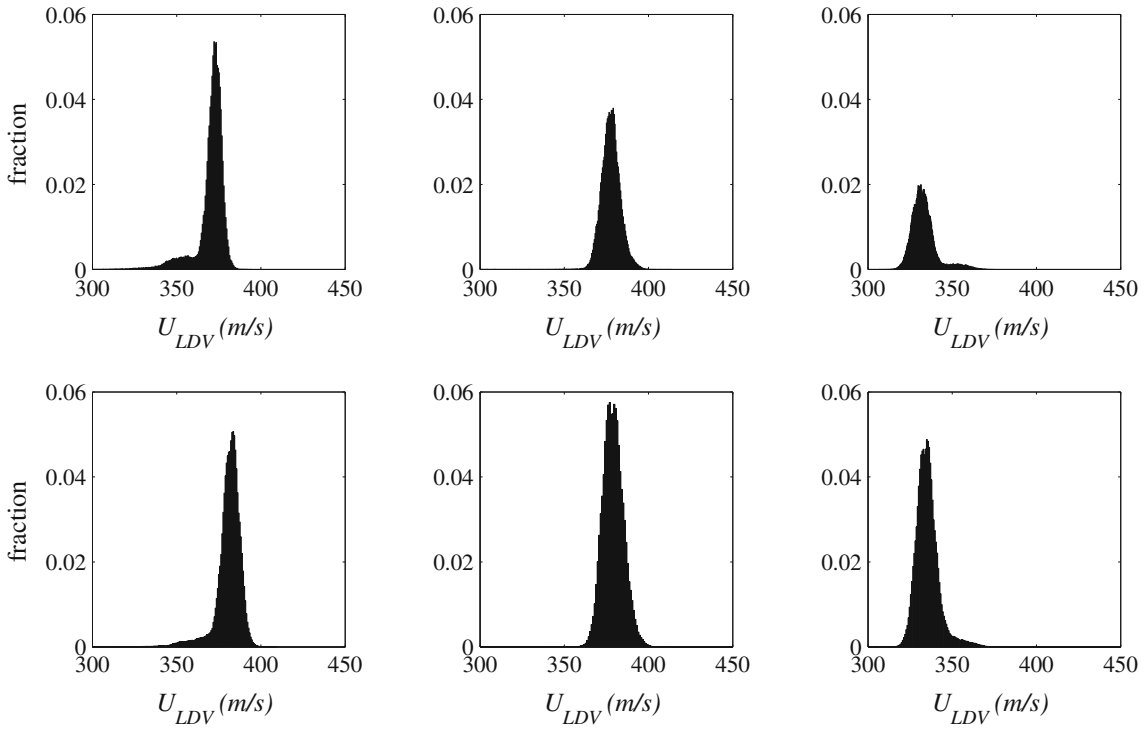


**Fig. 1** Histograms of axial velocity realizations at $x = 0.24D$ (*left* column), $x = 0.47D$ (*centre*) and $x = 0.63D$ (*right*) on the centreline, $M_j = 1.15$. *Top row* low photomultiplier feeding voltage ; *bottom row* high photomultiplier feeding voltage

low. For velocimetry applications, where the ratio of seeding particle density to fluid density is large, the drag force is dominant and the equation of motion greatly simplifies. Writing the equation in terms of space derivatives and projecting onto a flow direction leads to the following equation

$$\frac{1}{2}\frac{\mathrm{d}(U_{\mathrm{p}x}^2)}{\mathrm{d}x} = -\frac{3}{4}\, c_{\mathrm{D}}\, Re_{\mathrm{p}}\, \frac{\mu}{\rho_p d_{\mathrm{p}}^2}(U_{\mathrm{p}x} - U_{\mathrm{f}x}) \tag{1}$$

where $U_{\mathrm{p}x}$ and $U_{\mathrm{f}x}$ are the particle and flow velocities, respectively, projected on the $x$-axis, $c_{\mathrm{D}}$ is the drag coefficient, $\rho_p$ the particle density, and $d_{\mathrm{p}}$ the particle diameter. The particle Reynolds number $Re_{\mathrm{p}}$ is defined as

$$Re_{\mathrm{p}} = \frac{\rho\, \|\boldsymbol{U}_{\mathbf{p}} - \boldsymbol{U}_{\mathbf{f}}\|\, d_{\mathrm{p}}}{\mu} \tag{2}$$

where $\rho$ and $\mu$ are the fluid density and dynamic viscosity, respectively. Equation (1) is essentially the one commonly used in the literature [13,17,27]. In the following, the analysis is restricted to the centreline of nozzle and jet, where the axisymmetric geometry dictates that the fluid velocity and thus also the particle velocity have only an axial component. Subsequently, the projected components of Eq. (1) are the actual norms of the velocity vectors.

Many expressions exist for the drag coefficient $c_{\mathrm{D}}$. They are valid on different $Re_{\mathrm{p}}$ and $M_{\mathrm{r}}$ ranges, where $M_{\mathrm{r}}$ is the relative Mach number

$$M_{\mathrm{r}} = \|\boldsymbol{U}_{\mathbf{f}} - \boldsymbol{U}_{\mathbf{p}}\|/c \tag{3}$$

In Eq. (3), $c$ is the local speed of sound. The simplest expression of $c_{\mathrm{D}}$ is the Stokes' law, $c_{\mathrm{D}} = 24/Re_{\mathrm{p}}$, which applies when $Re_{\mathrm{p}}$ is smaller than unity [15], but this condition is too restrictive for the current applications. Walsh [26] reviewed and compared some expressions of the drag coefficient in light of experimental data and proposed a new formulation applicable to the case of low $M_{\mathrm{r}}$ values, writing

$$c_{\mathrm{D}} = c_{\mathrm{D,C}} + (c_{\mathrm{D,FM}} - c_{\mathrm{D,C}})\, \exp(-A \cdot Re_{\mathrm{p}}^N) \tag{4}$$

with $c_{\mathrm{D,C}}$, $c_{\mathrm{D,FM}}$, $A$ and $N$ parameters depending on $M_{\mathrm{r}}$.

When solving Eq. (1), the evolutions of $\rho$ and $\mu$ must be taken into account in the case of shock-containing jets. The density $\rho$ is deduced at each location from (1) the given Mach number (or also from the fluid velocity and the assumed total temperature) and (2) the local total pressure, using the perfect gas law. The viscosity $\mu$ is obtained by Sutherland's law

$$\mu = \mu_0\, (T/T_0)^{3/2}\, (T_0 + S)/(T + S) \tag{5}$$

where $T$ is the flow static temperature, $T_0$ a reference temperature and $S$ the Sutherland constant. The values of the constants $\mu_0$, $T_0$ and $S$ are taken from Pierce [21]. It should be noted that in a choked jet, it is possible that the total pressure might not be uniform. This issue will be addressed for each case analysed. Anyway, the influence of $\rho$ and $\mu$ on the final results has been checked to be small.

Two ways of solving the system formed by Eqs. (1), (2) and (4) are considered, depending on whether $U_{\mathrm{f}}$ or $U_{\mathrm{p}}$ is assumed. If $U_{\mathrm{f}}$ is assumed, $U_{\mathrm{p}}$ is integrated using the 4th order, 6 steps Runge–Kutta scheme by Berland et al. [4]. As a first application, the particle diameter is estimated in much the same way as in Yanta [27] or Ross et al. [23], by comparing numerical results of particle velocity to actual measurements. The comparison is performed for a subsonic jet at $M_{\mathrm{j}} = 0.9$. Here, the flow can be considered as isentropic throughout the nozzle and the jet potential core, so that no large error is done when considering that the local total pressure is the stagnation pressure. The one-dimensional isentropic flow hypothesis permits the flow velocity inside the nozzle to be obtained, knowing the internal geometry of the nozzle and the exit Mach number. In this subsonic case, the assumption is made that the flow velocity remains unchanged downstream of the nozzle exit, as it is expected inside the jet potential core. The particle velocity is then integrated inside the nozzle and in the jet plume, where it can be compared to the experimental data. The boundary conditions are such that $U_{\mathrm{p}}$ is taken equal to $U_{\mathrm{f}}$ at the beginning of the nozzle contraction. Postulated fluid velocity and integrated particle velocity for several guess values of $d_{\mathrm{p}}$ are given in Fig. 2a around the nozzle exit, located at $x/D = 0$. Increasing the particle diameter obviously induces a larger particle lag. As compared to $U_{\mathrm{f}} = 291.3\,\mathrm{m\cdot s^{-1}}$ in the nozzle exit plane, $U_{\mathrm{p}} = 288.5$, 285.7 and $282.9\,\mathrm{m\cdot s^{-1}}$ for $d_{\mathrm{p}} = 0.5$, 1.0 and $1.5\,\mu\mathrm{m}$, respectively. The experimental measurements are seen in Fig. 2b to compare well with the computed particle velocity for $d_{\mathrm{p}} = 1.0\,\mu\mathrm{m}$, which confirms the particle diameter stated in Sect. 2. Note that the velocity drop-off visible with increasing axial distance is not significant, corresponding to 1% of the maximum mean velocity over the four first jet diameters.

The system formed by Eqs. (1), (2) and (4) can also be solved knowing $U_{\mathrm{p}}$ and seeking $U_{\mathrm{f}}$. Firstly, the LDV experimental points are interpolated on a finer regular grid and a second-order central finite difference scheme is used to compute the space derivative in Eq. (1). Secondly, a Newton algorithm is used to find $U_{\mathrm{f}}$ from an initial guess value. This procedure yields an estimate of the flow velocity $U_{\mathrm{f}}$ within the jet plume starting from the measured particle velocity $U_{\mathrm{p}}$. It will be applied in Sect. 4.

## 4 Results and discussions

### 4.1 Structure of a $M_{\mathrm{j}} = 1.15$ jet

#### *4.1.1 Experimental results*

A gathering of the experimental results for the moderately underexpanded case of $M_{\mathrm{j}} = 1.15$ is presented in Fig. 3. The mean schlieren picture shows the well-known diamond

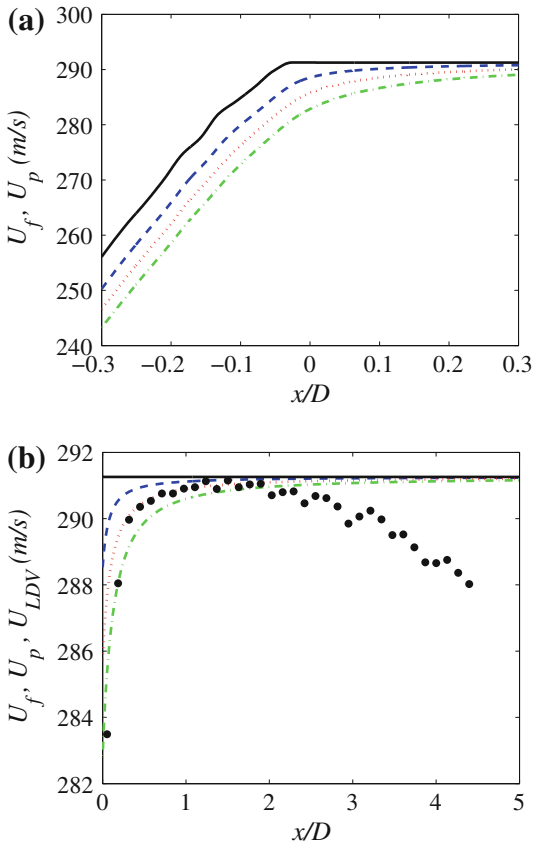


**Fig. 2** **a** Comparison between flow velocity $U_f$ and particle velocity $U_p$ for variable $d_p$ near the nozzle exit. **b** Comparison between computed $U_p$ and $U_{LDV}$. $M_j = 0.9$, $T_t = 32°C$. *Continuous lines* assumed $U_f$, *dashed lines* computed $U_p$ for $d_p = 0.5\,\mu m$, *dotted lines* computed $U_p$ for $d_p = 1.0\,\mu m$, *dashed-dotted lines* computed $U_p$ for $d_p = 1.5\,\mu m$. *Filled circles* LDV data points

shock-cell pattern. As can be seen from the velocity and static pressure measurements performed on the jet centreline (b), expansion occurs within the light right-pointing triangles of the schlieren image: the static pressure falls and the axial velocity increases. Conversely, compression takes place in the dark left-pointing triangles since $P_s$ increases and $U_{LDV}$ falls. This pattern is repeated until the end of the potential core (not visible here), where velocity and Pitot pressure start to fall for good. The axial velocity displays a local maximum at the junction between the light and dark zones of the schlieren picture and a local minimum at the 'shock' location. The Pitot pressure $P_p$ is displayed as measured and does not correspond to the jet local total pressure due to the shock forming ahead of the probe. It is seen to be almost uniform in both profiles, which is associated to a uniform total pressure at this moderate underexpansion. The static pressure curve is seen to oscillate about the ambient pressure in a slightly damped fashion, which is characteristic of the quasi-periodicity of the shock-cell structure. One may notice that the position of the $P_s$ local maximum in the first shock cell does not exactly correspond to that of the velocity minimum. This axial offset will be addressed in the following. It has to be emphasized that the shock-cell structure is weak, the shocks being no discontinuities but instead continuous modulation of the mean flow.

Axial traverses at a radial position $y = 0.25D$ from the centreline are also displayed in Fig. 3c. As before, the Pitot pressure is almost uniform. Static pressure and velocity data reveal however the short expansion phase through the fan attached to the nozzle lip and both variables remain nearly constant downstream until the entrance into the dark triangle of the first shock cell, as seen in the schlieren picture, where compression occurs. The existence of neutral external regions outside the light and dark triangles mentioned above has already been pointed out by Hu and McLaughlin [9] and Nouri and Whitelaw [19]. It has to be noted that the axial velocity on an off-axis traverse does not strictly correspond to the norm of the local velocity vector since the radial component is not accounted for. But measurements have shown that the magnitude of this latter component is very small compared to the axial component so that it is negligible in the velocity norm estimation.

The radial profiles of axial velocity at several downstream stations displayed in Fig. 4 permit a two-dimensional view of the jet to be gained. On these plots, the velocities corresponding to local Mach numbers of 1 and $M_j$ are marked by the horizontal lines to get an idea of the Mach number range of this jet. The local Mach number can be inferred from the LDV results if one assumes that the total temperature is uniform in the jet and equal to the reservoir temperature, by the formula

$$M = \left\{ \frac{U_{LDV}^2}{\gamma\, r\, T_t - U_{LDV}^2\,(\gamma - 1)/2} \right\}^{1/2} \tag{6}$$

where $M$ is the local Mach number, $\gamma = 1.4$ and $r = 287.06$ $J \cdot kg^{-1} \cdot K^{-1}$. The total temperature uniformity hypothesis was validated in [16] for supersonic shock-free jets. However, since the total temperature does not change across a shock, this assumption should hold in imperfectly expanded jets as well, at least in the potential core. Equation (6) can be rewritten so as to express $U_{LDV}$ against $M$, which then gives straightforwardly the velocity corresponding to any Mach number. As shown on the schlieren picture in Fig. 3, the three radial profiles have been measured in the expansion zone, in the middle of the first shock cell and in the compression zone. The upstream and downstream profiles look like similar plots in Nouri and Whitelaw [19], although their degree of underexpansion was higher than in the current study. Nonetheless, the absence of Mach disc in their jet allows us to compare both cases. In the expansion zone, Fig. 4a, where the centreline velocity increases, a velocity dip at the centre of the jet can be noticed. This is due to the fact that the expansion fans

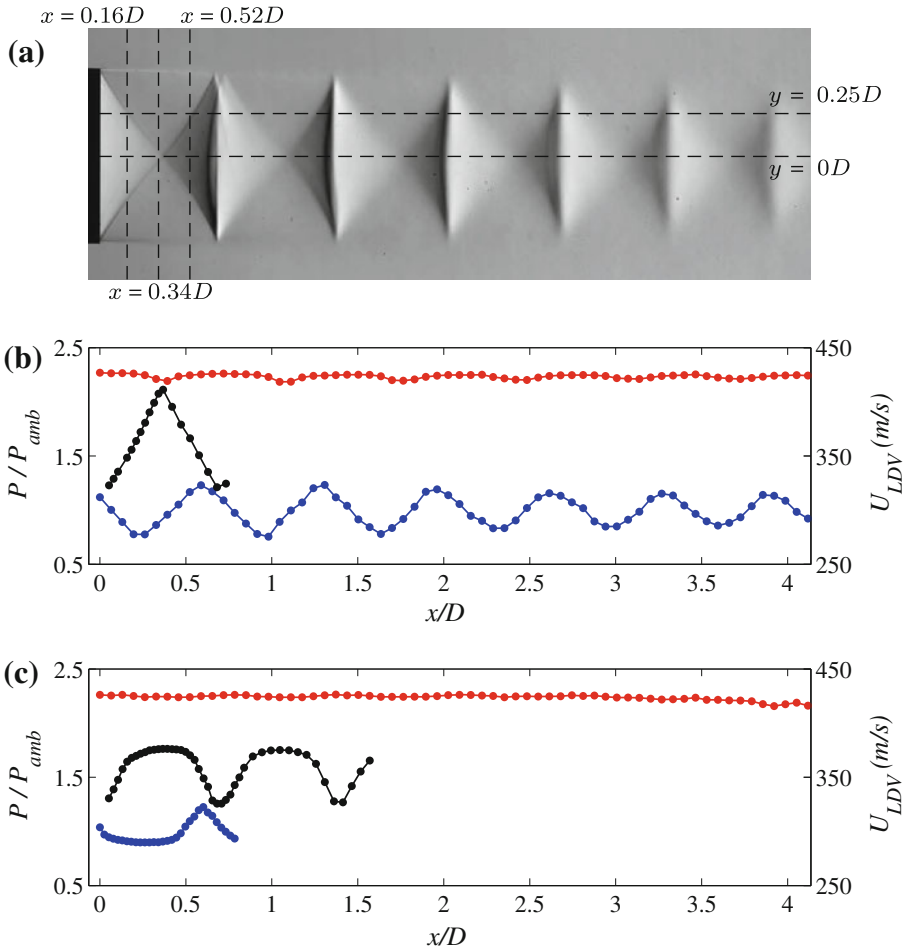


**Fig. 3** **a** Mean schlieren picture from 500 instantaneous frames (exposure time 9.4 µs) ; the *dashed lines* locate the displayed LDV profiles. **b** Axial traverses at $y = 0D$. **c** Axial traverses at $y = 0.25D$. *Blue circles* Static pressure, *red circles* Pitot pressure, *black circles* axial velocity. $P_{amb}$ is the ambient pressure

are attached to the lip so that their influence reaches the centreline further downstream. This means that the fluid acceleration occurs sooner in the outer part of the jet as compared to the centreline. Along the expansion zone (white triangle in the schlieren picture), the centreline velocity catches up with the outer velocity and finally moves past it. This explains the shape of the plot in Fig. 4b. In the compression zone (c), the velocity evolution is inverted as compared with the first half of the shock cell. The centreline velocity decreases first, leading to a very similar velocity profile as in the expansion zone.

It is worth noting that the neutral zones mentioned above are not regions of homogeneous flow with a static pressure being equal to the ambient. It is clear from Fig. 4 that the velocity varies a lot across these areas. The radial evolutions of the static pressure across them, not presented here, also display a strong change, which corresponds to density variations clearly visible in the data of Panda and Seasholtz [20]. However, almost no axial gradients are present inside the neutral regions, as it comes out from the off-axis velocity and pressure measurements shown in Fig. 3c. As the knife-edge is turned perpendicularly to the jet axis in the present study, only axial gradients can be visualised on the schlieren images, which explains why the neutral regions appear on the schlieren pictures like homogeneous regions, with intensity levels approximately equal to those of the still surroundings of the jet. These zones might be thought of as a stratified flow with pressure decreasing and velocity increasing toward the centreline.

It can be checked from the velocity marking corresponding to $M = 1$ that the flow is supersonic everywhere in the jet core (no particular attention has been given to the mixing layers in these traverses ; it is reminded that the jet surroundings have not been seeded so that the velocity measurements inside the mixing layers are biased). It is also interesting to note, as Seiner and Norum [25] did, that the local Mach number is very close to $M_j$ at the inner boundary of the mixing layer. This can be expected if one considers that the expansion from the stagnation pressure reigning inside the nozzle to the ambient pressure in the mixing layers is performed isentropically through the expansion fans so that the local Mach number at the inner boundary of the mixing layer is necessarily the fully expanded jet Mach number by definition.

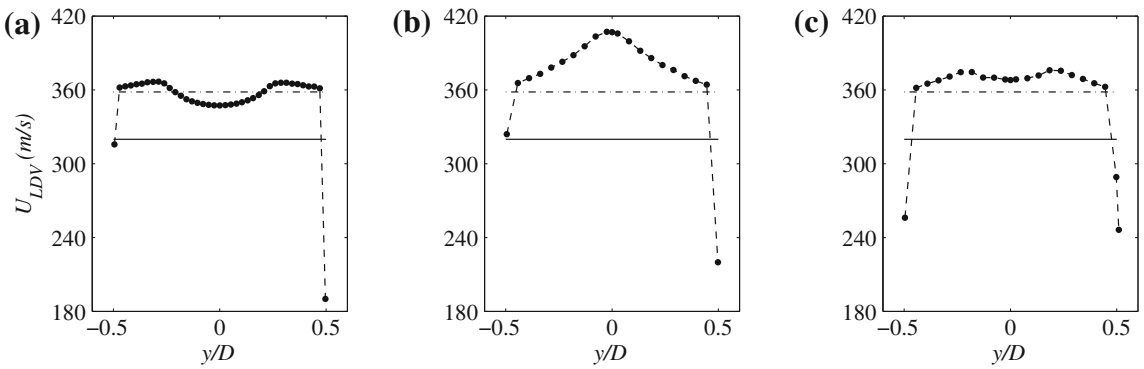


**Fig. 4** Radial profiles of the axial velocity in the first shock cell for $M_j = 1.15$. **a** $x = 0.16D$, **b** $x = 0.34D$, **c** $x = 0.52D$. *Filled circles* LDV data, *Continuous lines* velocity corresponding to $M = 1$, *dashed-dotted lines* velocity corresponding to $M = M_j$

#### 4.1.2 Estimation of the real flow velocity

The real flow velocity $U_f$ has been estimated by the procedure presented in Sect. 3.2. As mentioned there, the fluid density $\rho$ and dynamic viscosity $\mu$ are calculated for each trial value of $U_f$ at each grid step. To do so, the local total pressure is required. For the present case of $M_j = 1.15$, the variation of $P_t$ is small inside the jet plume so that the local total pressure can be considered to be the upstream stagnation pressure. For the computations, the values of the coefficients $c_{D,C}$, $c_{D,FM}$, $A$ and $N$ for $M_r = 0.1$ given by Walsh [26] are retained, since $M_r$ is smaller than 0.1 in the current case. The result of the procedure for the first shock cell is depicted in Fig. 5 and the following trends are suggested: $U_f$ is shifted upstream, by an amount of about $0.03D$ or 1.0 mm, as compared to $U_{LDV}$ and the amplitude of oscillation is somewhat larger than measured. This behaviour is caused by the particle lag. The maximum velocity goes from 411.2 to 427 m·s$^{-1}$ and the minimum from 321.1 to 310 m·s$^{-1}$, corresponding to less than 4 % deviation. This margin is in agreement with the accuracy estimate of 3 % stated by Ross et al. [23]. For this calculation, $M_r$ varies between 0 and 0.08 and $Re_p$ between 0 and 2 so that the postulated value of $c_D$ is validated a posteriori.

#### 4.1.3 Local Mach number estimations

The local Mach number $M$ has been estimated in two different ways. On the one hand, it has been assessed directly from the as-measured LDV data points, using Eq. (6). On the other hand, it has been computed from local $P_p$ and $P_s$ values using the Rayleigh–Pitot formula

$$\frac{P_p}{P_s} = \left[\frac{(\gamma+1)\,M^2}{2}\right]^{\gamma/(\gamma-1)} \left[\frac{\gamma+1}{2\gamma\,M^2-(\gamma-1)}\right]^{1/(\gamma-1)} \quad (7)$$

The hypothesis is made here that a normal shock forms ahead of the Pitot probe, which enables us to use the Rankine-Hugoniot normal shock relations. Corrections in $P_p$ measurement locations to account for the distance between normal shock and probe nose are insignificant in the present case and are not applied. Centreline and off-axis Mach number estimates from both methods are shown in Fig. 6. The first striking feature in both figures is the offset between LDV-based and pressure-based estimates. It is important to note that the downstream shift expected in the measured LDV data as compared to the actual fluid velocity profile, which is suggested by the analysis presented in Fig. 5 (and due to particle lag), is not sufficient to account for the 4.5 mm offset at hand. Offsetting the measured $P_s$ values by 4.5 mm yields the curves marked by triangles in Fig. 6. It is evident that the agreement between the two Mach number estimates has become very good through this modification. Thus, offsetting the $P_s$ traverse downstream can fix the problem. Moreover, it is reminded that an offset of the static pressure profile was already noticed in Fig. 3 as compared to the other experimental data. It has to be noted that the axial station of each static pressure value is taken as being the location of the tip of the probe, since the design by Pinckney [22] aims at recovering at the holes the static pressure existing at the tip. As a consequence, the following hypothesis is formulated.

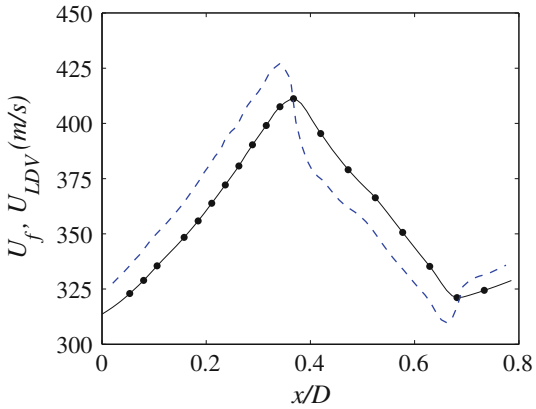


**Fig. 5** Estimation of the actual flow velocity $U_f$ from LDV data for $M_j = 1.15$. *Filled circles* LDV data points, *dashed line* $U_f$

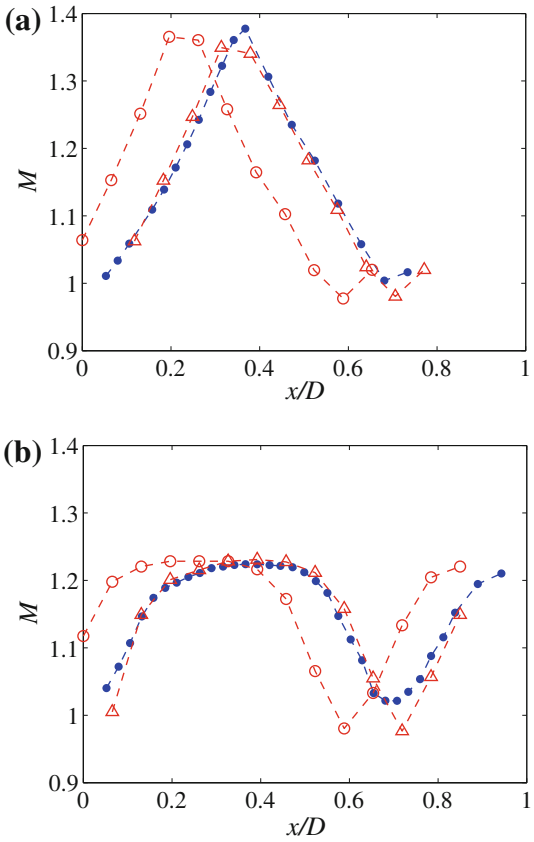


**Fig. 6** Mach number estimates from LDV and pressure measurements, $M_j = 1.15$. **a** Centreline profiles, **b** $y = 0.25D$. *Blue circles* velocity-based Mach number computation, *red circles* pressure-based computation from as-measured data, *red triangle* pressure-based computation with $P_s$ profile shifted by 4.5 mm downstream

However short the static probe is, it seems that the measured pressure is not the one prevailing at the tip but rather corresponds to the local pressure at some station next to the probe holes. Is is believed that such a situation could arise because of the high static pressure gradients existing in this type of flow, which do not exist in the original calculations by Pinckney [22]. A careful examination of the comparisons between measured and computed static pressure performed by Seiner et al. [24] shows that the measured shock locations are consistently ahead of the computed ones, which supports the above hypothesis. Furthermore, the authors of this paper also shift their profiles in the same fashion as is performed here, for their measurements with the lowest jet Mach numbers, arguing that the static probes are designed for higher local Mach numbers.

Turning back to Fig. 6, the magnitudes of the two Mach number estimates agree very well apart perhaps from the lower Mach number regions where the measured static pressure should not be as accurate [22]. The centreline Mach number (a) is seen to oscillate as expected about its ideally expanded value, going up to about $M = 1.4$, while the neutral zone of nearly constant Mach number is readily identified on the off-axis plot (b).

## 4.2 Structure of a $M_j = 1.50$ jet

### *4.2.1 Experimental results*

The highly underexpanded case of $M_j = 1.50$ is now examined. The first shock cell, featuring a Mach disc, is especially investigated. This normal shock is clearly visible in the shadowgram depicted in Fig. 7a, at an axial station $x$ slightly above $1D$. At the nozzle exit, the expansion fans attached to the lips and the associated widening of the jet diameter can also be observed. These features are characteristic of an underexpanded jet and are more obvious here than they were for $M_j = 1.15$. At the value of $M_j$ of interest, no strong barrel shock originating from the nozzle lips, as shown by Adamson and Nicholls [1] or by Fox [8], can be seen. Instead, the oblique faded lines originating from the nozzle lips seem to intensify into what is usually called intercepting shocks, upstream of the Mach disc. Such a picture is in agreement with the shadowgram of Eggins and Jackson [7], the computation of Katanoda et al. [10] or the very enlightening interferograms of Ladenburg et al. [11]. In the latter reference, these faded lines are described as 'valleys' and it is emphasized that they actually do not constitute shocks. Starting at the triple points of the Mach disc, the oblique reflected shocks are in contrast very obvious. Finally, note the presence of the slip lines, marking the separation between the subsonic flow immediately downstream of the Mach disc and the supersonic flow surrounding it.

The evolution of the velocity on the jet centreline and off axis are represented in Fig. 7b. Off axis, the axial velocity smoothly increases through the expansion fans attached to the nozzle lips, and reaches then a plateau of the same kind of that noticed at $M_j = 1.15$ (see Sect. 4.1). Across the reflected shock, the axial velocity decreases as expected. In the neutral zone and at the considered radial station, the local Mach number is seen to be close to, but slightly higher than, $M_j$. The presence of the normal shock is clear on the centreline profile, with the measured velocity going from 597 to 115 $\mathrm{m{\cdot}s^{-1}}$ within 2.5 mm. However, the axial velocity goes on decreasing long after the shock, for 10.5 mm. As it will be shown later, this is not believed to be entirely imputable to particle lag. This feature has already been observed by Eggins and Jackson [7] and is also supported by the density measurements of Ladenburg et al. [11] and Panda and Seasholtz [20], who showed that the density keeps increasing after the normal shock. The measured velocity just upstream of the Mach disc corresponds to a local Mach number of 2.64, which greatly exceeds $M_j$.

Some radial LDV profiles are displayed in Fig. 8. These results look similar to traverses presented by Eggins and

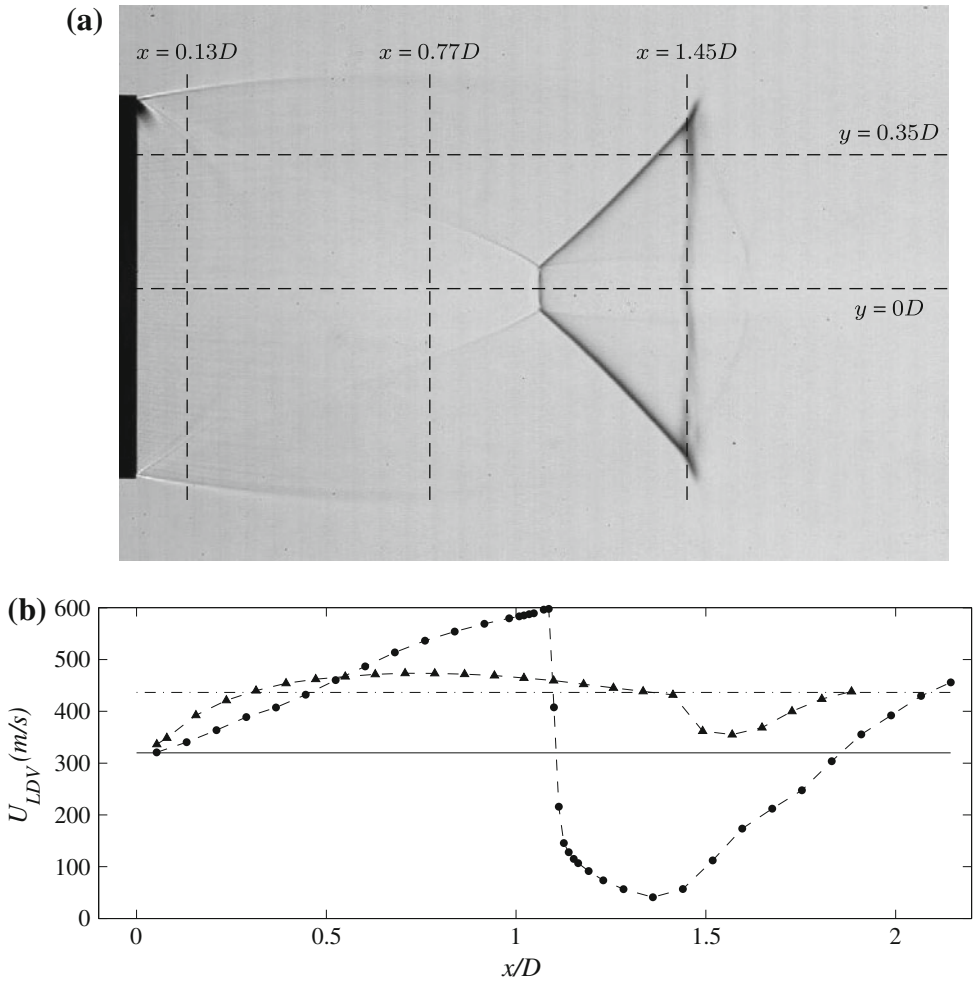


**Fig. 7** **a** Mean shadowgram from 500 instantaneous frames (exposure time 6.8 μs) ; the *dashed lines* locate the displayed LDV profiles. **b** Axial LDV profiles ; *filled circles* $y = 0D$, *filled triangles* $y = 0.35D$, *continuous line* velocity corresponding to $M = 1$, *dashed-dotted line* velocity corresponding to $M = M_j$

Jackson [7]. It stands out in the profile nearest to the nozzle exit (a) that the velocity increases much sooner in the outer parts of the jet than on the centreline, for the same reason as for $M_j = 1.15$. Further downstream but still upstream of the Mach disc (b), the situation is inverted with a larger centreline velocity. This arises from the continuous increase of the centreline velocity up to the Mach disc while off axis, the acceleration stops once the flow enters the neutral zones. Downstream of the Mach disc (c), the velocity is larger in an outer annulus surrounding the reflected shock, then decreases sharply through it and the slip line. Note that the difference between the minimum velocity on the jet axis and the velocity

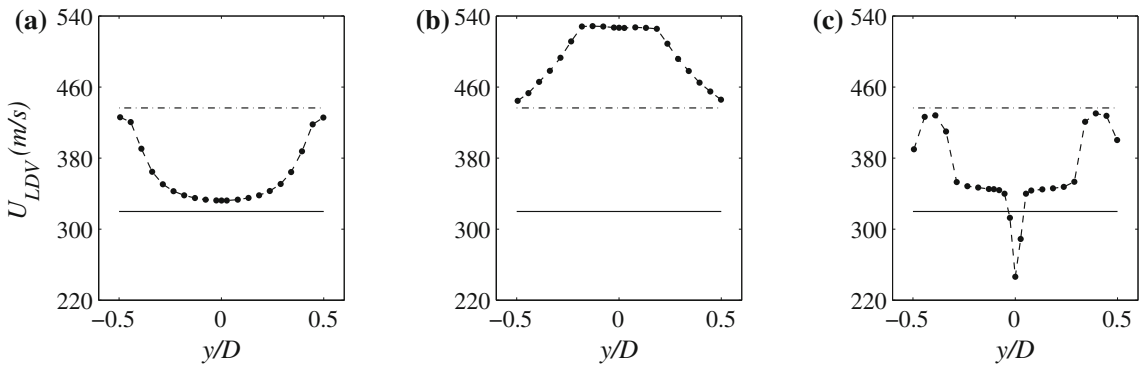


**Fig. 8** Radial profiles of the axial velocity in the first shock cell for $M_j = 1.50$. **a** $x = 0.13D$, **b** $x = 0.77D$, **c** $x = 1.45D$. *filled circles* LDV data, *continuous lines* velocity corresponding to $M = 1$, *dashed-dotted lines* velocity corresponding to $M = M_j$

measured at the same axial station during the centreline traverse (see Fig. 7b) probably arises from a small positioning inaccuracy. Considering the velocity markings corresponding to $M = 1$ and $M_j$, it is here again apparent, like for $M_j = 1.15$ in Fig. 4, that the local Mach number at the inner boundary of the mixing layer is very close to $M_j$.

#### 4.2.2 Estimation of the real flow velocity

Equation (1) can again be numerically integrated but the strong shock would have to be smoothed in order not to obtain oscillations in the result. This would then lead to a misrepresentation of the shock. To circumvent this difficulty, the relaxation distance of the particles behind the normal shock has been estimated. It is assumed that $U_f$ remains constant downstream of the Mach disc, and the minimum measured velocity of $41\,m\,s^{-1}$ is taken. It has to be noted that the normal shock relations lead to a larger velocity downstream of the disc, so that considering $41\,m\,s^{-1}$ is a conservative choice : the computed particle lag will be larger than in the real situation. $U_p$ is then integrated starting from the measured velocity at the shock location. The relative Mach number $M_r$ approaches 1.6 just downstream of the shock, so that the coefficients for $M_r = 1.6$ given by Walsh [26] are used for expressing $c_D$. They are not modified during the computation for simplicity, but it was checked that this also was a conservative choice. Finally, the total pressure value is taken as measured by a Pitot probe.

The resulting $U_p$ curve is shown in Fig. 9. Only 2 mm downstream of the shock, the particles have decelerated down to 97.5% of the velocity jump. It may be concluded that only in the few first millimetres after the shock is the measured velocity biased by the particle lag. The gradual velocity decrease observed for about 10.5 mm downstream of the Mach disc is therefore a real feature of the flow.

#### 4.2.3 Velocity fluctuations behind the Mach disc

Until now, only the mean velocity data have been analysed but the LDV also has the capacity to provide information on the turbulent fluctuations. The longitudinal velocity fluctuations measured on the jet axis at $M_j = 1.50$ are presented in Fig. 10 and show some interesting features. Firstly, the sharp peak slightly beyond $x/D = 1$ corresponds to the first measurement point behind the normal shock. This is a blatant sign of particle lag : each particle responds to the strong velocity gradient according to its size and the velocity histogram widens. Secondly, low fluctuation levels are reached just 2 mm downstream of the peak, long before the end of the mean velocity decrease, 10 mm downstream of the sharp fluctuation peak. This suggests that the effect of particle lag is limited to a small region behind the Mach disc, thus supporting the numerical results presented above. Thirdly, the fluctuation levels rise again further downstream, at an axial station coincident with the mean velocity re-increase downstream of the Mach disc. This strongly suggests that the acceleration leading to supersonic velocity sufficiently far downstream of the normal shock is due to turbulent momentum transfer occurring across the slip lines, as suggested by Katanoda et al. [10]. As it was quoted in this reference, the visualization by Yip et al. [29] shows the existence of large-scale turbulent structures along the slip lines. They are probably responsible for the high fluctuation levels measured on the jet centreline.

## 5 Conclusions

Two underexpanded free jets of fully expanded Mach numbers $M_j = 1.15$ and 1.50 have been studied experimentally. A LDV system has been set up and the health of

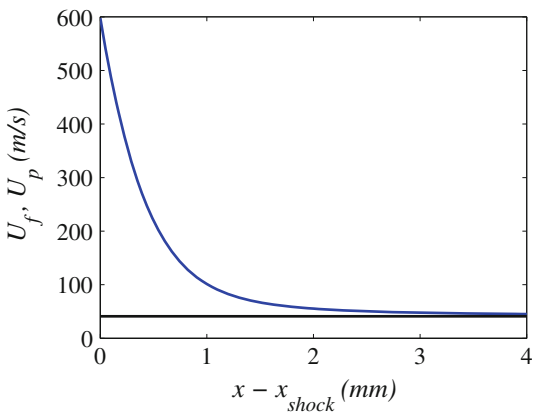


**Fig. 9** Tracer particle relaxation behind the Mach disc. *Black line* postulated constant $U_f$, *blue line* computed $U_p$ from $U_f$

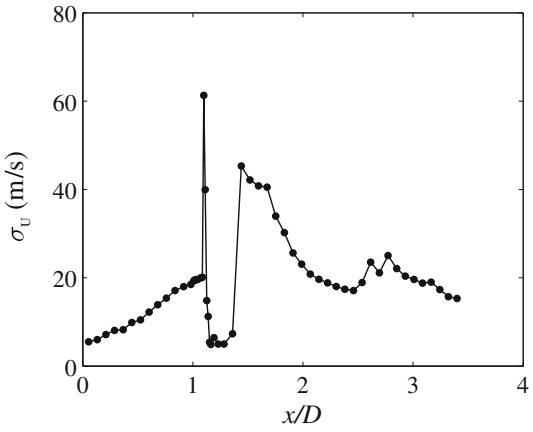


**Fig. 10** Longitudinal velocity fluctuations measured on the jet axis, $M_j = 1.50$. $\sigma_U$ is the root-mean-square fluctuating velocity

the measurements for these imperfectly expanded plumes has been checked by observing the velocity distribution histograms. The photomultiplier feeding voltage was raised near its limit value to diminish the effect of particle lag. Some thoughts have been given to this latter phenomenon, which is of considerable importance in a flow with strong velocity gradients. The equation of motion of the tracer particles in the flow have been solved. The particle size has been evaluated by integrating the particle velocity through the nozzle and the free jet and comparing it to a measured subsonic LDV profile. Moreover, the actual flow velocity inside the jet plume has been estimated using the same equation.

Pitot and static pressure measurements have been performed and compared, together with velocity profiles, to mean schlieren pictures in the moderately underexpanded case, at $M_j = 1.15$. This way, expansion and compression zones have been identified on the latter and all measured mean flow variables have been seen to smoothly oscillate about a global mean value, without actual shocks. Off-axis profiles have shown the existence of neutral regions of stratified, but not homogeneous, flow. Local Mach numbers have been separately estimated from pressure measurements and LDV data and a good agreement has been obtained, which substantiates the adequacy of the experimental techniques in the flows under consideration. The actual fluid velocity has been estimated and it has been observed as expected that the centreline LDV profile was shifted downstream as compared to the actual velocity and that the velocity extrema were less pronounced.

The dominant features of a highly underexpanded jet at $M_j = 1.50$ have been identified both on a shadowgram and on velocity profiles. The Mach disc obviously makes it hard for the tracer particles to follow the flow. Nevertheless, it has been observed after assessment of the particle relaxation distance downstream of the normal shock that the LDV permits the important trends of the flow to be faithfully obtained. Indeed, it has been shown that the gradual velocity decrease after the velocity jump associated with the Mach disc is relevant and does not come from particle lag.

**Acknowledgments** This research has been funded by the French Research Agency (Agence Nationale de la Recherche) through the ANR-10-BLAN-937-01 project JESSICA. The authors wish to thank Emmanuel Jondeau for his great help in setting up and performing the LDV experiments.

## References

1. Adamson, T.C., Nicholls, J.A.: On the structure of jets from highly underexpanded nozzles into still air. Report ERI Project 2397, The University of Michigan (1958)
2. Anderson, J.D.: Modern Compressible Flow with Historical Perspective, 2nd edn. McGraw Hill, New York (1990)
3. Barnet, D.O., Bentley, H.T.: Statistical bias of individual realization laser velocimetry. In: Proceedings of the 2nd International Workshop on Laser Velocimetry, pp. 428–444 (1974)
4. Berland, J., Bogey, C., Bailly, C.: Low-dissipation and low-dispersion fourth-order Runge-Kutta algorithm. Comput. Fluids **35**(10), 1459–1463 (2006)
5. Bridges, J.E., Wernet, M.P.: Turbulence associated with broadband shock noise in hot jets. NASA Technical Memorandum 215274 (2008)
6. Donaldson, C.D., Snedeker, R.S.: A study of free jet impingement. Part 1. Mean properties of free and impinging jets. J. Fluid Mech. **45**(2), 281–319 (1971)
7. Eggins, P.L., Jackson, D.A.: Laser-Doppler velocity measurements in an under-expanded free jet. J. Phys. D Appl. Phys. **7**(14), 1894–1907 (1974)
8. Fox, J.H.: On the structure of jet plumes. AIAA J. **12**(1), 105–107 (1974)
9. Hu, T.F., McLaughlin, D.K.: Flow and acoustic properties of low reynolds number underexpanded supersonic jets. J. Sound Vib. **141**(3), 485–505 (1990)
10. Katanoda, H., Miyazato, Y., Masuda, M., Matsuo, K.: Pitot pressures of correctly-expanded and underexpanded free jets from axisymmetric supersonic nozzles. Shock Waves **10**(2), 95–101 (2000)
11. Ladenburg, R., Van Voorhis, C.C., Winckler, J.: Interferometric studies of faster than sound phenomena. Part II. Analysis of supersonic air jets. Phys. Rev. **76**(5), 662–677 (1949)
12. Love, E.S., Grigsby, C.E., Lee, L.P., Woodling, M.J.: Experimental and theoretical studies of axisymmetric free jets. NACA Technical, Report R-6 (1959)
13. Maxwell, B.R., Seasholtz, R.G.: Velocity lag of solid particles in oscillating gases and in gases passing through normal shock waves. NASA Technical Note D-7490 (1974)
14. McLaughlin, D.K., Tiederman, W.G.: Biasing corrections for individual realization of laser anemometer measurements in turbulent flows. Phys. Fluids **16**(12), 2082–2088 (1973)
15. Melling, A.: Tracer particles and seeding for particle image velocimetry. Meas. Sci. Technol. **8**, 1406–1416 (1997)
16. Morrison, G.L., McLaughlin, D.K.: Instability process in low Reynolds number supersonic jets. AIAA J. **18**(7), 793–800 (1980)
17. Neilson, J.H., Gilchrist, A.: An analytical and experimental investigation of the trajectories of particles entrained by the gas flow in nozzles. J. Fluid Mech. **35**(3), 549–559 (1969)
18. Norum, T.D., Seiner, J.M.: Measurements of mean static pressure and far field acoustics of shock containing supersonic jets. NASA Technical Memorandum 84521 (1982)
19. Nouri, J.M., Whitelaw, J.H.: Flow characteristics of an underexpanded jet and its application to the study of droplet breakup. Exp. Fluids **21**(4), 243–247 (1996)
20. Panda, J., Seasholtz, R.G.: Measurement of shock structure and shock-vortex interaction in underexpanded jets using Rayleigh scattering. Phys. Fluids **11**(12), 3761–3777 (1999)
21. Pierce, A.D.: Acoustics: An Introduction to its Physical Principles and Applications. Acoustical Society of America, New York (1989)
22. Pinckney, S.Z.: A short static-pressure probe design for supersonic flow. NASA Technical Note D - 7978 (1975)
23. Ross, C.B., Lourenco, L.M., Krothapalli, A.: Particle image velocimetry measurements in a shock-containing supersonic flow. AIAA Paper 94–0047 (1994)
24. Seiner, J.M., Dash, S.M., Wolf, D.E.: Analysis of turbulent underexpanded jets, Part II : shock noise features using SCIPVIS. AIAA J. **23**(5), 669–677 (1985)
25. Seiner, J.M., Norum, T.D.: Experiments on shock associated noise of supersonic jets. AIAA Paper 79–1526 (1979)

26. Walsh, M.J.: Influence of particle drag coefficient on particle motion in high-speed flow with typical laser velocimeter applications. NASA Technical Note D-8120 (1976)
27. Yanta, W.J.: Measurements of aerosol size distributions with a laser Doppler velocimeter (LDV). AIAA Paper 73–705 (1973)
28. Yanta, W.J., Gates, D.F., Brown, F.W.: The use of a laser Doppler velocimeter in supersonic flow. AIAA Paper 71–287 (1971)
29. Yip, B., Lyons, M., Long, M., Mungal, M.G., Barlow, R., Dibble, R.: Visualization of a supersonic underexpanded jet by planar Rayleigh scattering. Phys. Fluids A **1**(9), 1449 (1989)